I.J. Intelligent Systems and Applications, **2026, 1, 119-131**
Published Online on February 8, 2026 by MECS Press (http://www.mecs-press.org/)
DOI: 10.5815/ijisa.2026.01.09

Enhanced MRI Segmentation and Severity Classification of Parkinson's Disease Using Hierarchical Diffusion-driven Attention Model

Redhya M.*
Department of Computer Applications, Kalasalingam Academy of Research and Education, Krishnankoil, Tamil Nadu, India
E-mail: redhya2414@gmail.com
ORCID iD: https://orcid.org/0000-0003-3897-8867
*Corresponding Author

M. Jayalakshmi
Department of Computer Science and Engineering, School of Computing, Kalasalingam Academy of Research and Education, Krishnankoil, Tamil Nadu, India
E-mail: jayalacsmi@gmail.com
ORCID iD: https://orcid.org/0000-0002-7297-9161

Rajermani Thinakaran
Faculty of Data Science and Information Technology, INTI International University, Nilai, Negeri Sembilan, Malaysia
E-mail: rajermani.thina@newinti.edu.my
ORCID iD: https://orcid.org/0000-0002-4026-3423

Received: 11 July 2025; Revised: 21 September 2025; Accepted: 26 November 2025; Published: 08 February 2026

Abstract: Early identification of Parkinson's disease (PD) from MRI remains challenging due to subtle structural alterations and the complexity of brain tissues. To address these challenges, this paper proposes a hierarchical framework termed Hierarchical Severity-Adaptive Diffusion Network, composed of three sequentially connected phases, where the output of each phase serves as input to the next for task-specific optimization. In the first phase, a graph diffusion-based convolutional network is employed to extract anatomical and structural features from multi-modal MRI data, enabling accurate segmentation of PD-relevant regions. Phase two introduces an edge-enhanced slice-aware recurrent network that incorporates Wiener filters and Sobel-based edge enhancement to reduce noise and partial volume effects while capturing structural continuity across adjacent MRI slices. Finally, for severity classification, non-linear severity-adaptive attention network is introduced, which emphasizes discriminative feature deterioration patterns across stages. This model uses Figshare PD dataset and demonstrates superior performance compared to established models like DenseNet121, VGG16, ResNet, MobileNet and Inception-V3, and achieves high accuracy (98.67), precision (0.99), recall (0.98), and F1 score (0.99), indicating its potential as an AI-assisted tool for PD severity assessment using MRI.

Index Terms: Parkinson's Disease, Disease Severity Classification, Diffusion Kurtosis Imaging, Substantia Nigra, Segmentation.

1. Introduction

Parkinson's disease (PD) is a progressive neurological disorder that results from the loss of dopamine-producing brain cells, leading to motor symptoms like bradykinesia, rigidity, tremors, and postural instability. MRI is a commonly used imaging technique in PD research, focusing on the substantia nigra (SN) and basal ganglia, which are critical for motor control. Advanced image processing enhances diagnostic accuracy and provides insights into disease progression [1-4]. However, segmenting these regions is challenging due to their small size, complex anatomy, and pathological changes. Techniques like region-based, atlas-based, and deep learning methods aid segmentation, but identifying disease-relevant features while minimizing artifacts remains difficult. Integrating multimodal imaging and time-series studies may improve diagnostic and prognostic tools [5-8].

MRI-based approaches for PD detection include diffusion tensor imaging (DTI) for white matter integrity, functional MRI for brain activity, susceptibility-weighted imaging for iron deposition, and structural imaging for atrophy. Despite their utility, these methods face challenges like subtle changes, overlapping symptoms with other neurodegenerative diseases, and data imbalance [9-12]. Machine learning techniques, including Random Forest, Support Vector Machines (SVMs), Artificial Neural Networks (ANNs), and Convolutional Neural Networks (CNNs), have been applied to classify PD stages and diagnose the disease. While CNNs excel at feature extraction, issues like insufficient labelled data and imbalanced datasets highlight the need for advanced analytical methods and multimodal approaches to enhance reliability and accuracy [13-15].

The arrangement of the paper is as follows. Section 2 provides a review of relevant literature; Section 3 delineates the methodology of the proposed system; Section 4 encompasses experiments, datasets and simulation output of the proposed system; Section 5 gives a discussion based on the comparison and evaluation approaches; and Section 6 offers suggestions for future enhancements and constraints of the approach.

2. Related Works

Iswarya et al. [16] explored five deep learning architectures to enhance MRI-based PD diagnosis, with three showing significant improvements and identifying a Deep Neural Network (DNN) as a suitable classification model. However, limited hyperparameter tuning and reliance solely on MRI restrict broader applicability. Sivaranjini et al. [17] utilized the AlexNet CNN architecture with transfer learning to classify PD and healthy controls using MRI, achieving accuracy but facing challenges with domain shifts and limited exploration of alternative architectures. Azadeh et al. [18] proposed a CNN model for staging PD, emphasizing supervised and unsupervised techniques but highlighting the need for ensemble methods to improve model robustness and expand diagnostic capabilities.

Camacho et.al. [19] developed and evaluated an explainable deep learning model for classification of PD from T1-weighted and diffusion-tensor MRI datasets using CNN and SmoothGrad saliency maps. This study revealed that DTI data are more important than T1-weighted data for classification. Nikhil et al. [20] trained a 3D CNN on T1-weighted MRI data from datasets like OASIS, ADNI, PPMI, and UPenn, testing performance with OASIS and UPenn datasets. Although radiomics features were extracted using a random forest baseline, reliance on MRI alone limited multimodal integration, and insufficient external validation hindered generalizability. Ya et al. [21] used structural MRI features and logistic regression to build models for cerebellar, subcortical, cortical, and composite regions, identifying potential neuroanatomical markers of PD. However, moderate AUC values suggest the models need further optimization and validation for clinical use.

Li et.al. [22] proposed an improved YOLOv5 detection algorithm with a CA attention module in backbone to find PD fuzzy lesion areas, a full-dimensional dynamic convolution in the Neck layer to enhance feature extraction and a decoupled head in Head layer to improve detection accuracy and reduce coupling. Although it helps in early detection of PD, limited number of participants (104) and lack of racial diversity statistics may affect the model's adaptability in wider population. Fu et.al. [23] used six ML models grounded in conventional T2W FLAIR images for screening PD in early stage. Radiomic features were extracted from SN, Red Nucleus, Globus Pallidus and Putamen regions of brain. As these regions were manually delineated by radiologists it was burdensome and resource-intensive, which at present can be done effectively with deep learning methods.

Based on the study, a novel approach, Hierarchical Severity-Adaptive Diffusion Network (HiSDN), is introduced in this paper integrating multimodal imaging for improved diagnostic accuracy and generalizability. This approach has three phases which is detailed in Algorithm 1:

- Graph Diffusion MRI-based Convolutional Network (GDM-CN): By integrating Diffusion Kurtosis Imaging (DKI) and Diffusion Basis Spectrum Imaging (DBSI) into a Graph Convolutional Network (GCN), captures intricate brain tissue microstructural changes, improving segmentation and feature precision for classification.
- Edge-enhanced Slice-Aware Recurrent Network (ESARN): Combines Wiener filtering and Sobel edge detection within a Graph Convolutional Recurrent Network (GCRN) to reduce blurring and enhance edge detection, improving the delineation of SN boundaries and increasing sensitivity in PD detection.
- Non-linear Severity-Adaptive Attention Network (NSAA-Net): Employs a VGG-based deep feature extractor followed by non-linear SVM classification and Support Vector Regression (SVR) to capture subtle MRI-derived variations, addressing symptom variability and improving the accuracy of PD severity classification.

3. Materials and Methods

Each phase of the proposed framework is implemented and trained independently and connected sequentially. GDM-CN improves segmentation accuracy by detecting subtle diffusion alterations and leveraging brain region relationships. This reduces misclassification errors and enhances diagnostic precision. ESARN is proposed for improved edge detection and reduced blurring. Additionally for classifying PD severity, NSAA-Net effectively detects motor and structural changes. This method ensures accurate classification into mild, moderate, and severe stages, handling symptom variability and advancing PD management. Architectural diagram of proposed HiSDN is illustrated in Fig.1.

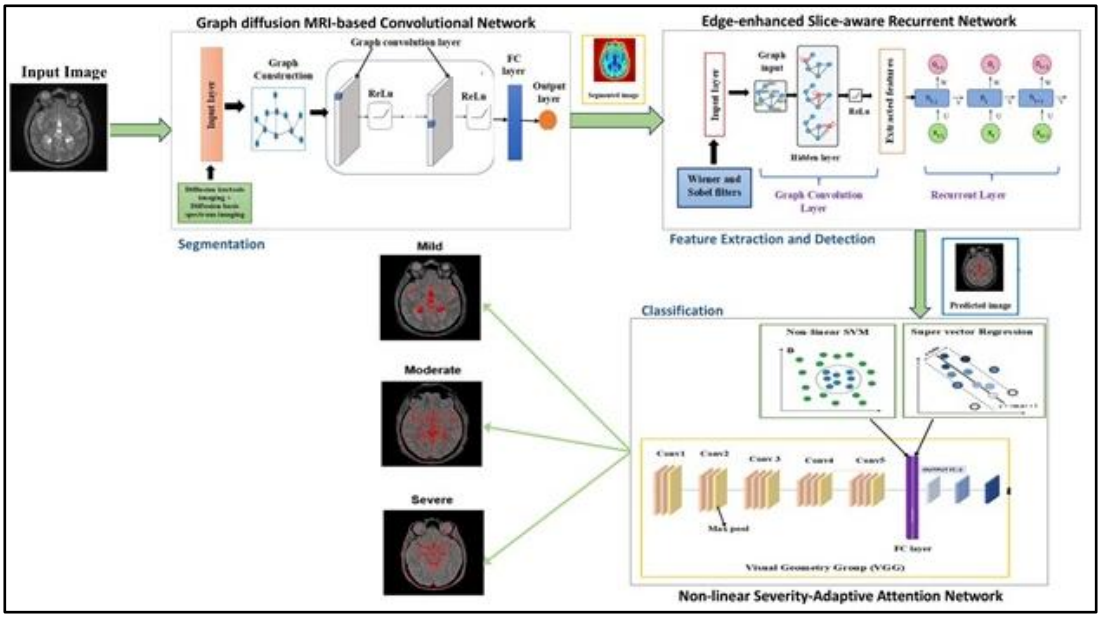

Fig.1. Architectural diagram of proposed HiSDN

3.1. Graph Diffusion MRI-based Convolutional Network

The flow diagram of GDM-CN is depicted in Fig.2. The input multi-modal MRI image is processed through a graph diffusion-based convolutional network to extract structural and anatomical features for accurate segmentation. DKI, an advanced diffusion imaging technique, captures non-Gaussian diffusion behavior by calculating kurtosis, which reflects tissue microstructural complexity. The DKI model is described by Equation (1)

$$\ln\frac{S(a,q)}{S_0} = -aD(q) + \frac{1}{6}a^2D(q)^2K(q) \tag{1}$$

where $S(a,q)$ - observed diffusion signal at gradient strength a and diffusion direction q, S_0 - baseline diffusion signal without gradients, $D(q)$ and $K(q)$ are the actual diffusion coefficient and actual kurtosis coefficient, respectively along direction $q = (q_1, q_2, q_3)$.

Metrics derived from DKI, such as Mean Kurtosis (M_K), axial kurtosis (A_K), and radial kurtosis (R_K), provide detailed tissue insights and are expressed in the following equations (2), (3) and (4)

$$M_K = \frac{1}{N}\sum_{i=1}^{N} K_i \tag{2}$$

$$A_K = K_1(\lambda_1) \tag{3}$$

$$R_K = \frac{K_2+K_3}{2} \tag{4}$$

where K_i are the kurtosis values across N diffusion directions and λ_1 - eigen value representing diffusivity in principal direction.

DBSI complements DKI by decomposing the diffusion signal into isotropic and anisotropic components for analyzing tissue heterogeneity. The measured form of the DBSI model is given in the following equation (5)

$$S_K = \sum_{i=1}^{N} f_i e^{-|\overrightarrow{a_k}|\lambda_{\perp i}} e^{-|\overrightarrow{a_k}|(\lambda_i-\lambda_{\perp i})cos^2\psi_{ik}} + \int_m^n f(D)e^{-|\overrightarrow{a_k}|D}d(D) \tag{5}$$

where S_K - observed diffusion signal for a voxel, f_i - fraction and $\lambda_{\perp i}$ - traverse diffusivity of i^{th} diffusion component, λ_i - axial diffusivity, ψ_{ik} - angle between k^{th} gradient direction and i^{th} diffusion tensor, $f(D)$ - isotropic diffusion spectrum and D - isotropic diffusivity ranging between m and n.

These metrics, including M_K, A_K, R_K and DBSI diffusion coefficients, serve as features for constructing a graph representation in GCN. Each node represents a brain region or voxel, while edges indicate spatial relationships. Graph convolution layers in the GCN extract hierarchical features using the following equation (6)

$$H^{(l+1)} = \sigma\left(\tilde{D}^{-\frac{1}{2}}\tilde{A}\tilde{D}^{-\frac{1}{2}}H^{(l)}W^{(l)}\right) \tag{6}$$

where $H^{(l)}$ - node feature matrix and $W^{(l)}$ - weight matrix at layer l, $\tilde{A}$ - adjacency matrix with self-loops, $\tilde{D}$ - degree matrix corresponding to $\tilde{A}$ and σ - activation function [24].

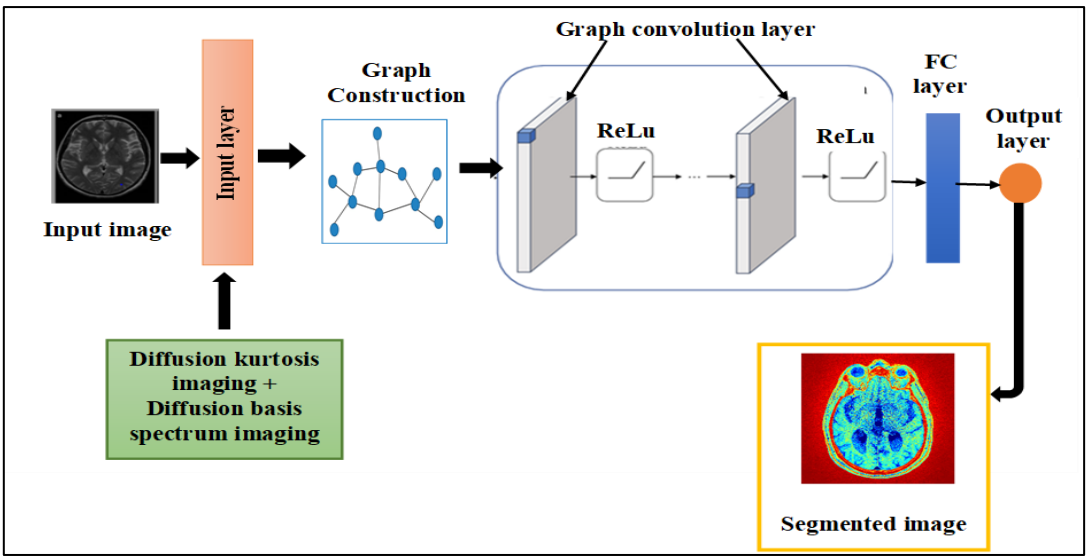

Fig.2. Flow diagram of GDM-CN

Nodes exchange information with their neighbours through the following equation (7)

$$H^{(l+1)} = \sigma\left(\sum_{j\in\mathcal{N}_i} \frac{1}{\sqrt{d_i d_j}} H_j^l W^{(l)}\right) \tag{7}$$

where $\mathcal{N}_i$ - neighbors of node i, and d_i, d_j - degrees of nodes i and j respectively.

After convolution, a pooling layer reduces the dimensionality of learned graph features, which are processed by fully connected layers for segmentation. The GCN's final layers produce output labels or probabilities for each voxel, delineating brain structures with high accuracy. By modelling both local and global diffusion characteristics, GCN significantly reduces misclassification errors and enhances segmentation performance.

3.2. Edge-enhanced Slice-Aware Recurrent Network

ESARN is a method designed to overcome the challenges in accurately segmenting SN from MRI, improve feature extraction and PD detection. As shown in Fig.3, ESARN integrates the spatial capabilities of GCNs with the inter-slice dependency modeling strengths of Recurrent Neural Networks (RNNs) within a GCRN. Segmented images isolating SN are represented as networks where nodes signify pixels and edges depict spatial relationships.

The Wiener and Sobel filters are applied before the convolutional layer to enhance image clarity. Wiener filter minimizes noise and reverses blurring by optimizing mean square error between actual and predicted signals. This reduces partial volume effects which occur when signals from multiple tissue types blur boundaries. Mathematically, Wiener Filter can be expressed as in equation (8).

$$\hat{f} = \mathcal{F}^{-1}\left(\frac{H^*}{|H|^2 + \frac{1}{N(f)}}\right) \tag{8}$$

where $\hat{f}$ - restored image, H - blurring filter, H^* - complex conjugate of H, $\mathcal{F}^{-1}$ - inverse Fourier transform and $N(f)$ - noise's power spectral density. This filtering enhances tissue boundaries, improving segmentation precision.

After that, Sobel filter is used, which determines the gradient of image intensity in both horizontal (G_a), and vertical (G_b) directions. Given an input image I with pixel coordinates (a, b), the gradients are computed using equations (9) and (10)

$$G_a = \begin{bmatrix} -1 & 2 & -1 \\ 0 & 0 & 0 \\ 1 & 2 & 1 \end{bmatrix} * I \tag{9}$$

$$G_b = \begin{bmatrix} -1 & 0 & 1 \\ 2 & 0 & 2 \\ -1 & 0 & 1 \end{bmatrix} * I \tag{10}$$

After calculating gradients, the gradient magnitude (G), representing edge strength, is derived using equation (11).

$$G(a,b) = \sqrt{{G_a}^2 + {G_b}^2} \tag{11}$$

where higher $G(a,b)$ values indicate stronger edges. Thresholding is applied to retain significant edges, aiding in delineating SN boundaries.

Next, the filtered images are processed through graph convolutional layers to extract hierarchical spatial features. For each slice index t, the graph convolution operation is expressed in the following equation (12)

$$K_t^{(m+1)} = \sigma\left(\tilde{D}^{-\frac{1}{2}}\tilde{B}\tilde{D}^{-\frac{1}{2}}K_t^{(m)}W^{(m)}\right) \tag{12}$$

where $K_t^{(m)}$ - feature matrix at layer m and slice t, $\tilde{B} = B + I$ is the adjacency matrix with additional self-loops, $W^{(m)}$ - learnable weight matrix at layer m, σ - non-linear activation function, and $\tilde{D}$ - degree matrix of $\tilde{B}$. By aggregating information from neighboring nodes, GCN effectively captures enhanced local spatial patterns, enhancing the discriminative power of the features. This is particularly effective for identifying spatial correlations in MRI data. The output of graph convolution layer K_t captures spatial features that incorporate both original voxel intensities and enhanced edge information.

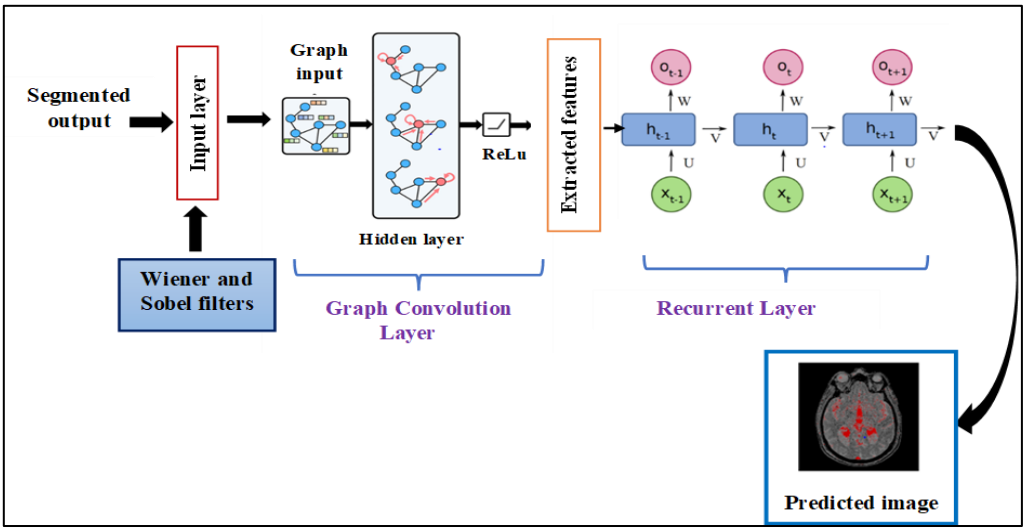

Fig.3. Architectural diagram of ESARN

After extracting spatial features, to capture inter-slice contextual dependencies, the ordered slice-wise feature matrix K_t is processed through a recurrent layer. The hidden state H_t at each slice index t is updated with equation (13)

$$H_t = tan\,h(W_H K_t + U_t H_{t+1} + B_H) \tag{13}$$

where W_H and U_t are the weight matrices for input features and previous hidden state respectively, B_H is the bias and $tanh$ is the activation function. The resulting hidden state encodes contextual dependencies across adjacent slices, reflecting structural variability across disease severity levels.

By applying Wiener and Sobel operations as a preprocessing step, ESARN addresses challenges like noise, partial volume effects, and edge delineation prior to feature learning. It effectively captures structural continuity across MRI slices, enhancing segmentation accuracy, sensitivity, and specificity. This makes ESARN a robust tool for reliable PD diagnosis and cross-sectional severity assessment.

3.3. Non-linear Severity-adaptive Attention Network

The architecture of NSAA-Net is illustrated in Fig.4. A unique feature of NSAA-Net is the usage of non-linear SVM and SVR in the fully connected layer of VGG. The VGG network is a deep CNN composed of multiple convolutional layers followed by pooling and fully connected layers. VGG effectively learns hierarchical representations of visual features, capturing subtle changes in motor control regions and cortical and subcortical structures.

In VGG, the detected image (X) undergoes multiple convolutional layers that apply learnable filters to extract features at various spatial scales. The convolution operation is shown in equation (14)

$$F_{j,k}^{l} = \sum_{p} \sum_{q} \sum_{r} W_{pq}^{l,c} \cdot X_{j+p,k+q,c} + B^{l} \tag{14}$$

where $F_{j,k}^{l}$ - feature map at spatial coordinates (j,k), $W_{pq}^{l,c}$ denoted as convolution filters, B^{l} - bias for layer l, $X_{j+p,k+q,c}$ - input pixel intensities with offsets p,q and input channel index c. After convolution, pooling layers reduce spatial dimensions while retaining important information. Max pooling retains the maximum value in each pooling region, ensuring robust feature extraction. These layers enhance the representation of subtle motor control changes for mild PD and cortical atrophy for severe stages. The flattened outputs from the pooling and convolutional layers are passed through fully connected layers, resulting in high-dimensional feature vectors.

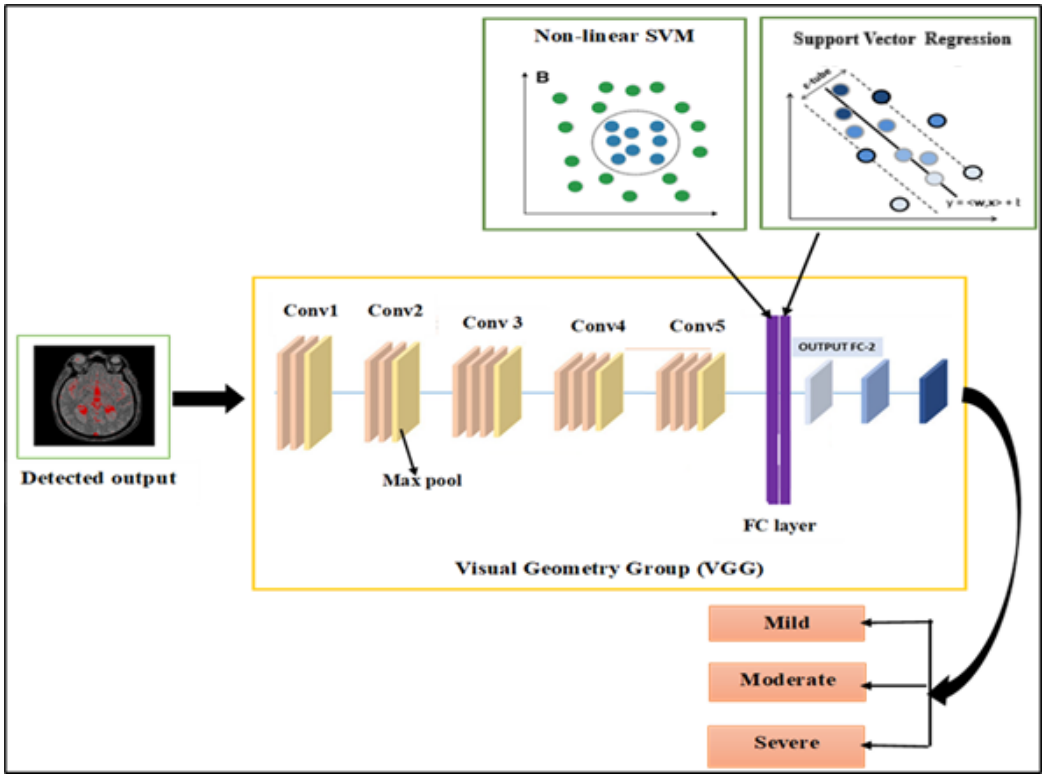

Fig.4. Flow diagram of NSAA-Net

The extracted features are fed into a non-linear SVM, which uses a kernel function to project features into a higher-dimensional space for improved separability. The kernel function is expressed in equation (15).

$$K(x_j, x_k) = exp\left(-\tau \left\| x_j - x_k \right\|^2\right) \tag{15}$$

where x_j and x_k are feature vectors and τ - scale parameter controlling decay rate of distance. The SVM identifies an optimized hyperplane [25] that separates PD severity into three classes: mild, moderate, and severe.

$$minimize \frac{1}{2}\|w\|^2 + C\sum_{j=1}^{N}(\xi_j + \xi_j^*) \qquad sub\ to\ y_j(w^T\phi(x_j) + b) \geq 1 + \xi_j,\ \ \xi_j \geq 0 \tag{16}$$

where, y_j - class labels with hyperplane weights w and bias b, $\phi(x_j)$ - feature mapping function and ξ_j, ξ_j^* - slack variables for soft margin. The SVM outputs class labels indicating the PD severity stages.

Simultaneously, the same feature vector is used for regression with SVR to predict a continuous PD severity score using equation (17).

$$f(x, \alpha_i, \alpha_i^*) = \sum_{i=1}^{N}(\alpha_i - \alpha_i^*)K(x_j, x_k) + B \tag{17}$$

where $f(x, a_i, a_i^*)$ - predicted severity score, $K(x_j, x_k)$ - kernel function, α_i, α_i^*- dual coefficients and B - bias. SVR captures variations in PD symptoms and ambiguities across stages, predicting a continuous severity score that reflects degeneration and structural atrophy.

Algorithm 1: Hierarchical Severity-Adaptive Diffusion Network

Input: Raw MRI images of the brain, Parameters for DKI and DBSI (e.g., diffusion directions, diffusion coefficients)

Phase 1: Graph Diffusion MRI-based Convolutional Network

Step 1: Preprocess the input MRI images.
Step 2: Compute DKI metrics using Equation (1)
Step 3: Compute DBSI parameters for each voxel.
Step 4: Construct a graph representation where Nodes represent brain regions (voxels) and Edges represent relationships between nodes.
Step 5: Apply graph convolution operations to extract hierarchical features using equation (5) and (6)
Step 6: Use pooling layers to reduce dimensionality.
Step 7: Generate segmentation output probabilities for each voxel.

Phase 2: Edge-enhanced Slice-Aware Recurrent Network

Step 8: Apply Wiener filtering to reduce noise and blurring using equation (7)
Step 9: Apply Sobel filtering to calculate horizontal (G_a) and vertical gradients (G_b) using Equations (8) and (9).
Step 10: Compute gradient magnitude to enhance edge detection using equation (10)
Step 11: Pass filtered images through the graph convolutional layer to capture spatial features per slice.
Step 12: Model inter-slice contextual dependencies using recurrent processing and update hidden states (H_t) using Equation (12)
Step 13: Enhanced delineation of SN boundaries.

Phase 3: Non-linear Severity-Adaptive Attention Network for classification

Step 14: Extract features from segmented images using the VGG architecture.
Step 15: Perform convolutional operations across multiple layers to extract hierarchical features.
Step 16: Apply max-pooling layers to reduce spatial dimensions while retaining critical information.
Step 17: Feed extracted features into a non-linear SVM:

i. Map features into higher-dimensional space using kernel function $K(x_j, x_k)$ in equation (15)
ii. Identify optimal hyperplane using Equation (16).

Step 18: Simultaneously, input the same feature vector into the SVR model.
Step 19: Predict a continuous severity score using equation (17)
Step 20: Combine outputs from SVM and SVR for final severity classification.

Output

- **Segmented MRI Images**: Clear delineation of SN.
- **Severity Classification**:
  - Labels indicating the stage of PD (mild, moderate, severe).
  - Continuous severity scores from SVR indicating disease severity.

The combined outputs of the non-linear SVM and SVR provides a thorough evaluation of PD severity. The classification labels from SVM indicate the disease stage, while the continuous severity scores from SVR offer a detailed measure of disease severity. Thus, improving accuracy, sensitivity, and specificity, enabling precise categorization of PD stages.

4. Results

This part includes the results obtained from the proposed model and the performance of the proposed system. The hardware setup for implementing the proposed system is Intel i5 processor with 8GB RAM and Windows 10 (64 bit) operating system. The proposed system is simulated in Python. The hyperparameters of the proposed model and its values are shown in Table 1.

Table 2 explains the feature score values of the proposed model. M_K measures non-Gaussian diffusion behaviour, indicating tissue microstructure complexity. A_K captures diffusion restrictions along the primary direction, highlighting water movement abnormalities. R_K represents diffusion limitations in perpendicular direction, often due to tissue heterogeneity. The Sobel Filter Gradient Magnitude quantifies edge strength in brain structures, aiding precise segmentation. The SVM Classification Score gives a probability score for disease severity classification, while the SVR Predicted Severity Score provides a continuous measure, predicting PD severity. Together, these features enhance the model's ability to capture both structural changes and disease severity effectively.

Table 1. Hyper parameters and its values

Hyper parameter	Value
Learning Rate	0.001
Batch Size	32
Epochs	50
Size of the convolution Kernel Size	3x3
Size of the pooling kernels	2x2
Dropout Rate	0.5
Regularization (L2)	0.01
Number of neurons in the output layer	3 (mild, moderate, severe)
SVM function kernel	Non-linear

Table 2. Feature score values and its range

Feature	Range
Mean Kurtosis (M_K)	0.1 - 2.5
Axial Kurtosis (A_K)	0.1 - 1.5
Radial Kurtosis (R_K)	0.05 - 1.2
Sobel Filter Gradient Magnitude	0 - 255
SVM Classification Score	0.0 - 1.0
SVR Predicted Severity Score	0 - 100

4.1. Dataset Description

The PD dataset used in this study is publicly available on Figshare, contains multi-modal MRI images from 71 subjects. Due to the absence of subject-level identifiers and site or temporal metadata, the data were split into training, validation, and test sets at the image level. Accordingly, the reported results are interpreted as cross-sectional performance indicators rather than definitive measures of clinical generalization. The dataset can be accessed from the following link: https://doi.org/10.6084/m9.figshare.30999604

4.2. Simulation Output of the Proposed Model

This section interprets and analyses an effective simulation modeling strategy of the proposed HiSDN for PD Detection and Classification model. DKI and DBSI are applied to the original scan which highlights the fine details and subtle changes in the brain's microstructure, offering a more comprehensive view compared to the original scan. Fig.5 expresses the segmented image. The colors in this image represent different segments, where each color corresponds to a particular region or tissue type within the brain.

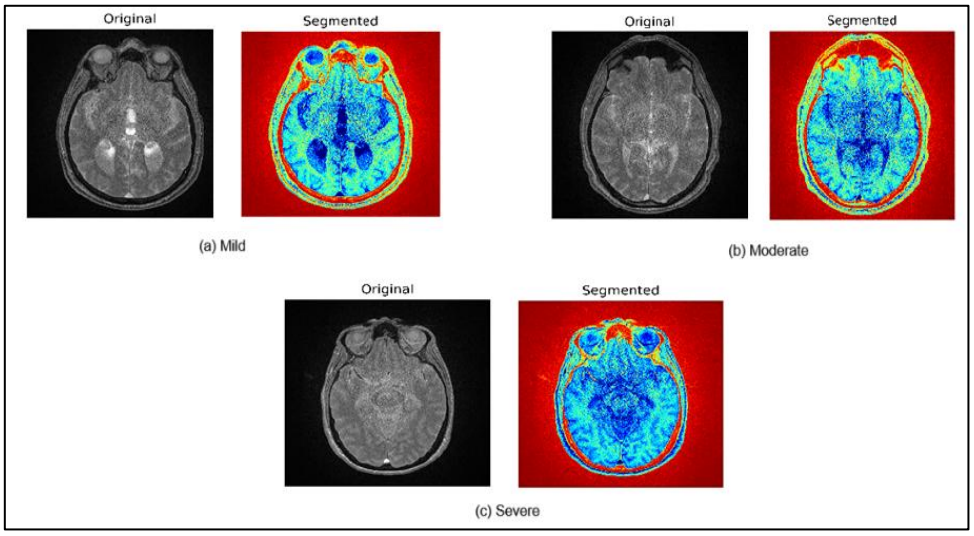

Fig.5. Segmented image of (a) mild (b) moderate (c) severe

The predicted image of (a) mild (b) moderate (c) severe is shown in Fig.6. This highlighted areas in red indicate the regions identified by the model, possibly showing anomalies, or other areas relevant to a diagnosis.

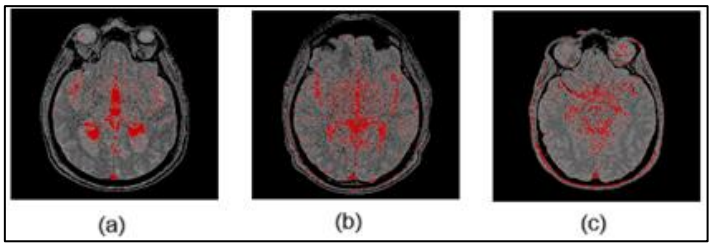

Fig.6. Predicted image of (a) mild (b) moderate (c) severe

The Fig.7(a) illustrates the training and validation accuracy of the proposed model. Performance metrics were calculated per scan on the held-out test set using image-level data partitioning. Training accuracy rises from below 0.80 to about 0.95, while validation accuracy starts above 0.80, peaks near 0.90, and stabilizes with minor fluctuations, indicating potential overfitting. Fig.7(b) shows training loss dropping sharply in early epochs, reflecting rapid learning, while validation loss decreases initially but fluctuates, suggesting variable generalization. However, its fluctuations suggest variability in performance on unseen data.

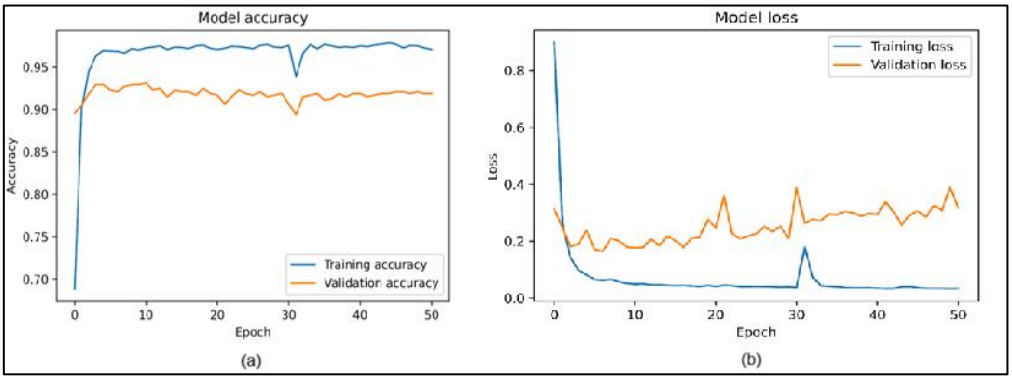

Fig.7. (a)Training and validation accuracy (b) Loss of the proposed model

5. Discussion

The results of this study indicate that the proposed HiSDN approach significantly enhances the accuracy and reliability of PD detection and severity classification. This section examines the achieved outcomes, comparing them with existing models across various metrics, and discuss the implications, advantages, and limitations of the proposed approach.

5.1. Performance of the Proposed Model

This section provides an analysis of the experimental results for the proposed HiSDN model in classifying PD severity using MRI scans. Metrics such as accuracy, recall, precision, sensitivity, specificity, f1-score, ROC, and AUC were used to evaluate performance. The model achieved its highest accuracy of 0.99 at 50 epochs and a minimum of 0.45 at 10 epochs, attributed to enhanced border detection and the ability to capture PD-related structural variability across disease severity levels. Fig.8 shows the suggested model's accuracy performance.

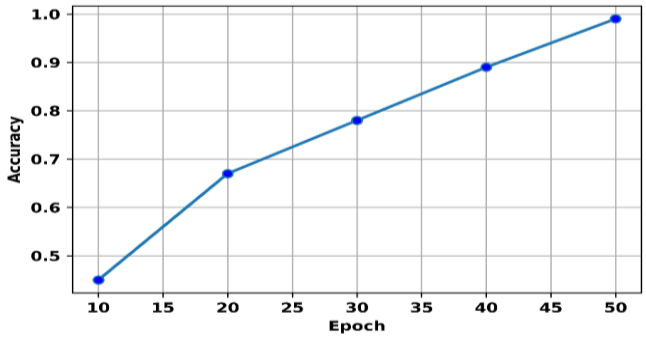

Fig.8. Accuracy of the proposed model

To obtain a more robust assessment and minimize bias associated with single data splits, 5-fold cross-validation was conducted. Table 3 shows the K-fold cross validation performance of the proposed model across the five folds. This model achieved an average accuracy of 98.67% with mean precision, recall and f1-score of 98.64%. The consistent performance across folds indicates stable generalization across different data partitions. Owing to the absence of subject-level identifiers, evaluation was performed at the image level, and the results should therefore be interpreted as cross-sectional classification performance rather than patient-level diagnostic accuracy. Further validation on patient-level and multi-site datasets is planned to assess clinical generalizability.

Table 3. K-Fold cross validation performance of the proposed system

Fold (K)	Accuracy (%)	Precision (%)	Recall (%)	F1-score (%)
K = 1	98.81	98.75	98.78	98.76
K = 2	98.47	98.43	98.43	98.43
K = 3	98.30	98.29	98.29	98.29
K = 4	99.15	99.12	99.12	99.12
K = 5	98.64	98.60	98.60	98.60
Average	98.67	98.64	98.64	98.64

An ablation study was conducted to quantify the contribution of each phase in the proposed framework which is shown in Table 4. Using only diffusion-based segmentation (Phase 1) yields an accuracy of 92.77% which indicates that segmentation alone is insufficient for robust severity classification. Incorporating edge-enhanced slice-aware features (Phases 1 and 2) improves the performance to 94.43% showing the added value of inter-slice feature refinement. When Phase 1 is excluded and only Phases 2 and 3 are employed, accuracy increases to 97.12%, highlighting the importance of severity-adaptive classification. Adding a standard VGG-based feature extractor further boosts accuracy to 98.14%, confirming the complementary role of deep feature representation. The complete framework achieves the highest performance (98.67%), confirming that each phase contributes incrementally and that the observed gains are not driven by a single component alone.

The model's AUC reached 0.99, shown in Fig.9(a), enhanced by VGG's comprehensive feature extraction and non-linear SVM's precise classification. Mean squared error (MSE) reduced significantly, achieving 0.05 at 50 epochs compared to 0.32 at 10 epochs, shown in Fig.9(b), indicating improved feature extraction accuracy. Loss values ranged from 0.01 to 0.045, shown in Fig.9(c), with the NSAA-Net minimizing prediction errors by effectively capturing complex patterns and relationships in the data.

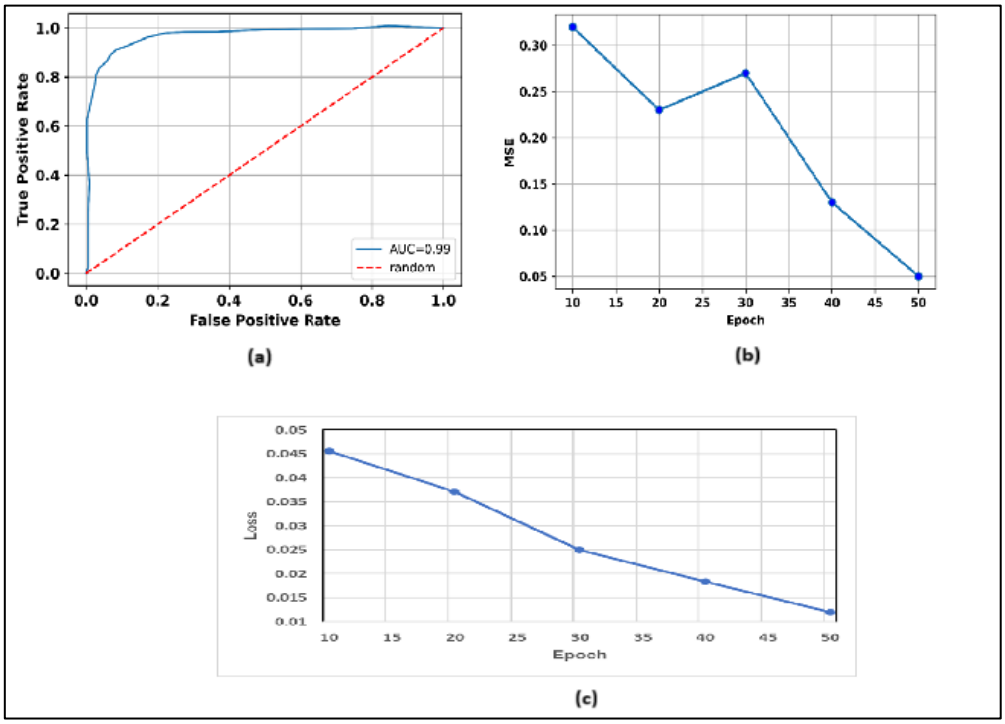

Fig.9. Proposed model's (a) AUC (b) MSE (c) Loss

Table 4. Ablation study of the proposed system

Configuration	Phase1: Diffusion-based Segmentation	Phase 2: Edge-enhanced Slice-aware Features	Phase 3: Severity-adaptive Classification	Accuracy (%)	Precision (%)	Recall (%)	F1 – score (%)
Phase 1 only	✓	✗	✗	92.77	92.69	92.63	92.62
Phase 1 + Phase 2	✓	✓	✗	94.43	94.26	94.26	94.26
Phase 2 + Phase 3	✗	✓	✓	97.12	97.06	97.08	97.07
Phase 1 + Phase 2 + VGG	✓	✓	✓	98.14	98.13	98.13	98.13
Full Proposed Framework	✓	✓	✓	**98.67**	**98.64**	**98.64**	**98.64**

5.2. Comparison of the Proposed Model

This section describes in detail the achieved outcome by comparing it with existing models and displaying their results based on various metrics like accuracy, recall, precision and F1-score. It also highlights the proposed HiSDN approach for PD classification with the traditional models.

Comparison of proposed model's various metric values with existing models [13] such as DenseNet121, VGG16, ResNet, MobileNet and Inception-V3 is illustrated in Table. 5. The proposed model outperforms these existing models, which attains a highest precision value of 0.987, recall value of 0.986, F1-score value of 0.986 and AUC value of 0.99.

Table 5. Comparison of various metrics of the proposed model with existing models

Model	**Precision**	**Recall**	**F1-score**	**AUC**
DenseNet121	0.865	0.9	0.798	0.907
VGG16	0.793	0.886	0.798	0.829
ResNet	0.88	0.769	0.798	0.882
MobileNet	0.86	0.902	0.802	0.902
InceptionV3	0.817	0.844	0.798	0.827
Proposed	0.987	0.986	0.986	0.99

Overall, a comparison between the suggested methodology and the existing approaches is presented in this section using graphs and tables. Results show that HiSDN achieves higher accuracy, precision, recall, and lower computation time compared to previous techniques. Despite its significant advancements, the limitation of the proposed approach is that it requires high-quality diffusion imaging data and substantial computational resources, which may not be available in all clinical settings. This study is limited to image-level analysis on a single public MRI dataset that lacks subject-level identifiers, healthy controls, and confounding parkinsonian conditions, and therefore provides only preliminary cross-sectional evidence, necessitating future patient-level, multi-site studies to establish clinical generalizability.

6. Conclusions

The approach Hierarchical Severity-Adaptive Diffusion Network presents a novel solution for classifying PD severity, addressing limitations in existing methods. By integrating DKI and DBSI into the GCN framework, the approach enhances segmentation by capturing detailed microstructural brain changes. ESARN improves boundary clarity by reducing blurring and enhancing edge detection, while NSAA-Net uses VGG derived features with non-linear SVM and SVR for effective PD severity classification.

Compared to models like VGG16, ResNet, Inception-V3, and Xception, the proposed method achieves superior metrics, including a specificity and sensitivity of 0.98, precision of 0.987 and AUC of 0.99. It also minimizes loss (0.01) and MSE (0.05). This hierarchical model demonstrates significant advancements in PD classification by combining robust segmentation and classification techniques. Overall, the proposed method can be positioned as an AI-assisted decision-support tool within radiology workflows, complementing MRI-based assessment by highlighting disease-related structural patterns and supporting severity evaluation.

Acknowledgment

We wish to thank Dr. Robert Mathew, Chief Neurologist, Professor and Head, Department of Neurology, Sree Mookambika Institute for Medical Sciences for sharing important details related to this work.

Declaration of Competing Interest

The authors affirm that they have no known financial or interpersonal conflicts that would have appeared to have an

impact on the research presented in this study.

References

[1] Minervini, G., Franco, R., Marrapodi, M.M., Ronsivalle, V., Shapira, I. and Cicciù, M. Prevalence of temporomandibular disorders in subjects affected by Parkinson disease: A systematic review and metanalysis. J. Oral Rehabil. 50:877–885, 2023. https://doi.org/10.1111/joor.13496

[2] Camacho, M., Wilms, M., Mouches, P., Almgren, H., Souza, R., Camicioli, R., Ismail, Z., Monchi, O. and Forkert, N.D. Explainable classification of Parkinson's disease using deep learning trained on a large multi-center database of T1-weighted MRI datasets. NeuroImage Clin 38:, p.103405, 2023. https://doi.org/10.1016/j.nicl.2023.103405

[3] Li, C., Hui, D., Wu, F., Xia, Y., Shi, F., Yang, M., Zhang, J., Peng, C., Feng, J. and Li, C. Automatic diagnosis of Parkinson's disease using artificial intelligence base on routine T1-weighted MRI. Front Med 10:. p.1303501, 2024. https://doi.org/10.3389/fmed.2023.1303501

[4] Beheshti, I. and Ko, J.H. Predicting the occurrence of mild cognitive impairment in Parkinson's disease using structural MRI data. Front Neurosci 18:. p.1375395, 2024. https://doi.org/10.3389/fnins.2024.1375395

[5] Ariz, M., Martínez, M., Alvarez, I., Fernández-Seara, M.A., Castellanos, G., Catalonian Neuroimaging Parkinson's Disease Consortium, Pastor, P., Pastor, M.A. and Ortiz de Solórzano, C. Automatic Segmentation and Quantification of Nigrosome-1 Neuromelanin and Iron in MRI: A Candidate Biomarker for Parkinson's Disease. J Magn Reson Imaging, 2023. https://doi.org/10.1002/jmri.29073

[6] Basukala, D., Mukundan, R., Lim, A., Hurrell, M.A., Keenan, R.J., Dalrymple-Alford, J.C., Anderson, T.J., Myall, D.J. and Melzer, T.R. Automated segmentation of substantia nigra and red nucleus using quantitative susceptibility mapping images: Application to Parkinson's disease. Comput Electr Eng 91:., p.107091, 2021. https://doi.org/10.1016/j.compeleceng.2021.107091

[7] Nahar, N., Ara, F., Neloy, M.A.I., Biswas, A., Hossain, M.S. and Andersson, K. Feature Selection Based Machine Learning to Improve Prediction of Parkinson Disease. In: Lecture Notes in Computer Science (including subseries Lecture Notes in Artificial Intelligence and Lecture Notes in Bioinformatics). Springer Science and Business Media Deutschland GmbH, pp 496–508, 2021. https://doi.org/10.1007/978-3-030-86993-9_44

[8] Xiong, Y. and Lu, Y. Deep Feature Extraction from the Vocal Vectors Using Sparse Autoencoders for Parkinson's Classification. IEEE Access 8:27821–27830, 2020. https://doi.org/10.1109/ACCESS.2020.2968177

[9] Khanna, K., Gambhir, S. and Gambhir, M. Current challenges in detection of parkinson's disease. *JOURNAL OF CRITICAL REVIEWS*, *7*(18), pp.1461-1467, 2020. https://www.researchgate.net/publication/357870234

[10] Zhang, J. Mining imaging and clinical data with machine learning approaches for the diagnosis and early detection of Parkinson's disease. npj Park. Dis. 8, p.13, 2022. https://doi.org/10.1038/s41531-021-00266-8

[11] Lee, J.Y., Martin-Bastida, A., Murueta-Goyena, A., Gabilondo, I., Cuenca, N., Piccini, P. and Jeon, B. Multimodal brain and retinal imaging of dopaminergic degeneration in Parkinson disease. Nat Rev Neurol 18:201–220, 2022. https://doi.org/10.1038/s41582-022-00618-9

[12] Kurmi, A., Biswas, S., Sen, S., Sinitca, A., Kaplun, D. and Sarkar, R. An Ensemble of CNN Models for Parkinson's Disease Detection Using DaTscan Images. Diagnostics 12:., p.1173, 2022. https://doi.org/10.3390/diagnostics12051173

[13] Basnin, N., Nahar, N., Anika, F.A., Hossain, M.S. and Andersson, K. Deep learning approach to classify Parkinson's disease from MRI samples. In *International conference on brain informatics* (pp. 536-547). Cham: Springer International Publishing, 2021. https://doi.org/10.1007/978-3-030-86993-9_48

[14] Redhya, M., & Sathesh Kumar, K. Refining PD classification through ensemble bionic machine learning architecture with adaptive threshold based image denoising. *Biomed Signal Process Control 85:*, 2023. https://doi.org/10.1016/j.bspc.2023.104870

[15] Ahmed, I., Aljahdali, S., Khan, M.S. and Kaddoura, S. Classification of parkinson disease based on patient's voice signal using machine learning. Intell Autom Soft Comput 32:705–722, 2022. https://doi.org/10.32604/iasc.2022.022037

[16] Veetil, I.K., Gopalakrishnan, E.A., Sowmya, V. and Soman, K.P. Parkinson's Disease Classification from Magnetic Resonance Images (MRI) using Deep Transfer Learned Convolutional Neural Networks. In: Proceedings of the 2021 IEEE 18th India Council International Conference, INDICON 2021. Institute of Electrical and Electronics Engineers Inc., 2021. https://doi.org/10.1109/INDICON52576.2021.9691745

[17] Sivaranjini, S. and Sujatha, C.M. Deep learning based diagnosis of Parkinson's disease using convolutional neural network. Multimed Tools Appl 79:15467–15479, 2020. https://doi.org/10.1007/s11042-019-7469-8

[18] Mozhdehfarahbakhsh, A., Chitsazian, S., Chakrabarti, P., Chakrabarti, T., Kateb, B. and Nami, M. An MRI-based deep learning model to predict Parkinson's disease stages. *medRxiv*, pp.2021-02, 2021. https://doi.org/10.1101/2021.02.19.21252081

[19] Camacho, M., Wilms, M., Almgren, H., Amador, K., Camicioli, R., Ismail, Z., Monchi, O., & Forkert, N. D. Exploiting macro- and micro-structural brain changes for improved Parkinson's disease classification from MRI data. Npj Parkinson's Disease, 10(1), 2024. https://doi.org/10.1038/s41531-024-00647-9

[20] Dhinagar, N.J., Thomopoulos, S.I., Owens-Walton, C., Stripelis, D., Ambite, J.L., Ver Steeg, G., Weintraub, D., Cook, P., McMillan, C. and Thompson, P.M. 3D convolutional neural networks for classification of Alzheimer's and Parkinson's disease with T1-weighted brain MRI. In *17th International Symposium on Medical Information Processing and Analysis* (Vol. 12088, pp. 277-286). SPIE, 2021. https://doi.org/10.1101/2021.07.26.453903

[21] Ya, Y., Ji, L., Jia, Y., Zou, N., Jiang, Z., Yin, H., Mao, C., Luo, W., Wang, E. and Fan, G. Machine Learning Models for Diagnosis of Parkinson's Disease Using Multiple Structural Magnetic Resonance Imaging Features. Front Aging Neurosci 14:. p.808520, 2022. https://doi.org/10.3389/fnagi.2022.808520

[22] Li, H., Yang, Z., Qi, W., Yu, X., Wu, J., & Li, H. Parkinson's image detection and classification based on deep learning. BMC Medical Imaging, 24(1), 2024. https://doi.org/10.1186/s12880-024-01364-8

[23] Fu, J., Chen, H., Xu, C., Jia, Z., Lu, Q., Zhang, H., Hu, Y., Lv, K., Zhang, J., & Geng, D. Harnessing routine MRI for the early screening of Parkinson's disease: a multicenter machine learning study using T2-weighted FLAIR imaging. Insights into Imaging, 16(1), 2025. https://doi.org/10.1186/s13244-025-01961-3

[24] Wang, Q., Li, L., Qiao, L., & Liu, M. Adaptive Multimodal Neuroimage Integration for Major Depression Disorder Detection. Frontiers in Neuroinformatics, 16, 2022. https://doi.org/10.3389/fninf.2022.856175
[25] Jain, V., Singh, R., & Gupta, A. Exploring Binary Classification Models for Parkinson's Disease Detection. Procedia Computer Science, 235, 2332–2341, 2024. https://doi.org/10.1016/j.procs.2024.04.221

Authors' Profiles

Redhya M. is a researcher in the Department of Computer Applications (MCA) at Kalasalingam Academy of Research and Education (KARE). Her research interests include medical image analysis, deep learning–based disease detection, and AI-driven decision support systems, with a focus on neurodegenerative disorders and has published her work in peer-reviewed journals and conference proceedings.

Dr. M. Jayalakshmi is an Associate Professor in the Department of Computer Science and Engineering (CSE) at Kalasalingam Academy of Research and Education (KARE). She holds her Ph.D. degree in Computer Science and Engineering from Anna University. Her research interests focus on intelligent edge computing for IoT, AI-driven decision systems, and cybersecurity. She has contributed to several edited volumes and peer-reviewed conference proceedings in these areas.

Dr. Rajermani Thinakaran is an Associate Professor and Senior Lecturer in the Faculty of Data Science & Information Technology at INTI International University, Nilai, Malaysia. She holds a PhD in Computer Science from Universiti Teknologi Malaysia (UTM). Her research areas include artificial intelligence, Assistive Tech, eLearning and Gaming, and has published extensively in international journals and conference proceedings.

How to cite this paper: Redhya M., M. Jayalakshmi, Rajermani Thinakaran, "Enhanced MRI Segmentation and Severity Classification of Parkinson's Disease Using Hierarchical Diffusion-driven Attention Model", International Journal of Intelligent Systems and Applications(IJISA), Vol.18, No.1, pp.119-131, 2026. DOI:10.5815/ijisa.2026.01.09